Alternating Current Electrospraying

Siddharth Maheshwari, Nishant Chetwani, and Hsueh-Chia Chang*

Center for Microfluidics and Medical Diagnostics, Department of Chemical and Biomolecular Engineering, University of Notre Dame, Indiana 46556

Electrospraying has attracted the attention of many researchers, ranging from analytical chemists to physicists, not only because of the rich physics associated with it, but also due to its wide-ranging applicability. Therefore, considerable research has been devoted to exploring this interfacial phenomenon. However, there still are areas of electrospraying that have remained unexplored. Until recently, significantly less effort had been directed toward electrospraying with an alternating current (ac) electric field in comparison to electrospraying with direct current (dc) field. This article comes as an attempt to summarize the work done on ac electrospraying in the authors' group. A classification of this behavior into different frequency domains is provided, with an underlying mechanism that leads to physical features distinct from dc electrospraying. Potential uses of ac electrospraying, which cannot be realized by its dc counterpart, are also discussed.

Electrospraying is a method to generate fine aerosols by the application of a high potential difference across a liquid filled capillary. In contrast to other commonly used atomization techniques like two fluid nozzle atomization or compressed gas atomization, electrospraying can produce a very fine aerosol of monodisperse drops. Additionally, due to the charging of the liquid phase by the electric field, the charged drops break into even finer droplets, finally leading to gas phase ion generation. This particular characteristic of the electrosprays has been appropriately utilized to ionize the large, nonvolatile biomolecules like DNA and proteins in the mass spectrometry toward drug discovery research.[1] Apart from biological applications, electrosprays are widely used for industrial applications such as precise coating and polymer deposition on substrates.[2] The small volume of the drops generated with electrospraying makes it a very efficient tool for nanotechnology as well, allowing the dispersion and delivery of nanomaterials. All these applications have employed dc (direct current) electrospraying, i.e. a dc potential has been used to create the necessary electric field. Given the time-invariant nature of a dc electric field, dc spraying exhibits a steady behavior. On the contrary, modifying the forcing function by introducing an ac (alternating current) frequency alters the characteristic steadiness of electrospraying and provides an additional parameter for control. In this review, we discuss the departure of ac electrospraying from dc behavior and highlight its key features. We begin by providing a brief overview of dc electrospraying in the next section.

1. DC Electrospraying

When a thin metal capillary, $\sim 10{-}100 \mu$m in diameter, filled with a liquid is charged to a sufficiently high dc potential of several kilovolts, the liquid meniscus that protrudes from the end of the capillary deforms into a conical shape known as the Taylor cone. A thin and steady liquid jet emanates from the tip of this conical meniscus, which subsequently breaks up to form charged drops in the submicron range. This method of electrohydrodynamic atomization, commonly known as dc electrospraying, has been the subject of extensive study, particularly because of its applicability in electrospray ionization mass spectrometry, drug encapsulation, electrospinning, coating tech-

nology, etc.[2] One of the earliest reported works in electrospraying dates back to 1914 by John Zeleny.[3]

The mechanism behind the formation of a conical meniscus and the generation of charged drops is well-known.[4-7] In response to the applied potential, charge separation in the liquid takes place; co-ion accumulation at the meniscus tip can then occur by interfacial tangential conduction. The electric field has a $1/\sqrt{r}$ scaling with respect to the radial coordinate r obtained by balancing the capillary forces (only the azimuthal capillary pressure, since the axial capillary pressure in a cone is identically zero) with the Maxwell pressure. The Maxwell pressure is the electrical stress defined as $\varepsilon E^2/2$, where ε is the permittivity and E is the electric field. Hence, the Maxwell pressure that scales as $1/r$ offsets the azimuthal capillary pressure σ/r for any r, where σ is the surface tension. Such an exact balance of forces for all r is fundamentally responsible for the selection of the Taylor cone, which contains a continuous range in r and hence has no selected length scale.

Once a conical shape is formed and adequate co-ion accumulation occurs such that the resulting repulsive force due to the charge buildup is sufficient to overcome the surface tension of the drop meniscus, a thin liquid jet, whose dimension depends upon conductivity and liquid flow rate, erupts from the conical tip. The emanating jet breaks up into drops which possess net charge. As the drops evaporate in-flight, thereby reducing their mass, the charge density increases and results in Rayleigh fission of the drop once the surface tension holding the drop together is exceeded by charge repulsion. As a consequence, the drops successively decrease in size. The charge of the drops from dc electrosprays has the same polarity as the needle electrode and can be selected by imposing the proper potential on the electrode.

In dc electrospraying, it is therefore clear that the charges in the drops originate from the charge separation and accumulation that takes place in the liquid meniscus. This is also clear from the observation that if a low conductivity fluid such as ethanol or liquid paraffin is used as the working fluid, the conductivity must be enhanced by seeding the fluid with additives, if spraying is to be observed. Evidently for this steady cone-jet mode, the charge relaxation time $\beta\varepsilon_0/K$ needs to be much smaller as compared to the hydrodynamic time LR^2/Q such that the free charges are confined to a thin layer near the cone surface and the bulk is quasi-neutral. Here, L and R are the axial and radial

---

* To whom correspondence should be addressed. E-mail: hchang@nd.edu.

length scales in the jet, Q is the liquid flow rate, β and K are the dielectric constant and conductivity of the liquid, respectively, and ε_0 is the permittivity of free space. Hence, when the flow rate Q is higher than the critical flow rate, given by $Q_c \sim LR^2K/\beta\varepsilon_0$, the bulk no longer remains quasi-neutral. For typical length scale of $L \sim 1$ mm and $R \sim 1$ mm, the value of critical flow rate for dodecanol[8] ($K = 2.85 \times 10^{-6}$ S/m and $\beta = 6.5$) is approximately 5×10^{-5} m^3/s while for dioxane + 66% water ($K = 1.3 \times 10^{-3}$ S/m, and $\beta = 49.1$), it is roughly 3×10^{-3} m^3/s. Outside these limits, some form of jetting has also been observed, but with very different voltage-spray characteristics to those of the classical Taylor cone.[9] Also, if the charge accumulation at the tip is to be sustained, the interfacial field must have a significant tangential component, particularly for semiconducting liquids.

2. AC Electrospray

In contrast to the well-understood field of dc spraying, there have been relatively few studies on spraying trends under an ac electric field. The few studies available have been with either at low frequencies or dc superimposed ac fields.[10,11] Behavior analogous to a changing dc field has been reported. The cones are formed and terminated every half-cycle. There have been reports where distinct behavior as compared to traditional electrospraying was reported,[12] but there has been no consistent experimental and mechanistic investigation regarding the effect of ac electric field on electrospraying. We found that there is rich parametric space that has been hitherto unexplored. There are two, very distinct, phenomena seen at low (<10 kHz) and high frequencies (>10 kHz).

2.1. Low Frequency Behavior. At low frequencies, liquid phase charge separation and accumulation behavior, analogous to dc type behavior is possible and nontrivial drop shapes and dynamic electrosprays can be excited. But besides charge separation, resonant vibration can also be induced at specific low frequency ac fields, since the natural vibration frequency of the drop and its overtones can coincide with the applied frequency. In addition, an ac-induced Maxwell force on an electrode exhibits a maximum at a frequency near the inverse charging time due to a diffuse layer screening effect.[13] Hence, by using microdrops and low ac frequency such that the latter matches the drop resonant frequency and the diffuse layer charging time, we observe resonating polyhedral drops which give rise to multiple transient Taylor cones on the interface with increase in voltage.

The experimental setup resembles conventional dc spray experiments. A sinusoidal ac signal can be generated by a function/arbitrary waveform generator (Agilent 33220A) and magnified through a radio frequency (RF) amplifier (Powertron 250 A) and a secondary high voltage transformer (Industrial Test Equipment, 0.1−10 kHz), capable of delivering up to 10 000 V$_{p-p}$. A steel microneedle is filled with the working fluid and mounted obliquely with an angle of 45° to the horizontal plane such that a nanoliter sized drop could be extracted from it. If necessary, the needle inlet was connected to a syringe pump for supplying liquid at a predetermined rate. The counter electrode consisted of a stripe of copper tape placed 10 mm away from the needle tip. The applied voltage and frequency were monitored by a high voltage ac probe (Tektronix, P6015A) linked with an oscilloscope. The entire phenomenon was imaged by an inverted microscope (Olympus IX-71) and recorded using a high speed camera (Olympus i-speed) at 500−6000 frames/s.

For microdrops with dimensions smaller than the capillary length $R_c = (\sigma/\rho g)^{1/2}$, approximately 1.5 mm for acetonitrile,
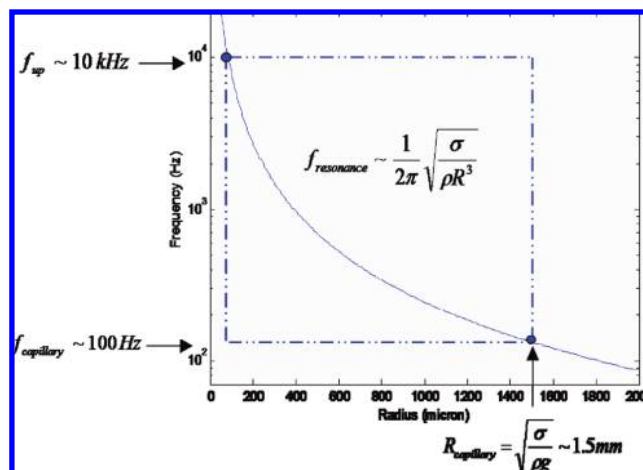
Figure 1. Radius−frequency diagram, illustrating the frequency window of resonant vibration. Rayleigh dispersion relation is plotted showing the size variation with frequency. The segment of the line between f_{up} and $R_{capillary}$ denotes the resonance regime that can be observed experimentally.

gravitational effects are negligible, and the resulting spherical drops with a radius R possess discrete resonant frequencies. The resonant modes exhibit the following resonant frequencies given by the Rayleigh−Lamb (RL) dispersion relationship for the inviscid case,

$$f_n = \frac{1}{2\pi}\sqrt{\frac{n(n-1)(n+2)\gamma}{\rho R^3}} \qquad \text{(i)}$$

where the integer n ($n \neq 1$) indicates the polar wavenumber. We also note that this is independent of the azimuthal wavenumber, m.[14] The fundamental frequency at $n = 1$ is $2\pi f_1 = (\sigma/\rho R^3)^{1/2}$, corresponding to an isolated sphere. The fundamental frequency f_1 is plotted vs R in Figure 1 for acetonitrile that allows us to design the appropriate resonant experiments.

There are, however, constraints that impose specific windows on the drop size and the correlated ac frequency f through (i). The upper bound on R is for a sphere with a radius equal to the capillary length R_c, the corresponding resonant frequency f_c is about 150 Hz. Above this radius, gravity dominates and severe liquid dripping occurs to prevent the formation of a spherical drop. The lower bound on R is imposed by an upper bound on f via induced-charge polarization mechanism.[15] As there is a finite charge accumulation time for the diffuse layer polarization at the liquid−air interface, the applied frequency has this upper cutoff. From an experimental perspective, a frequency of ∼10 kHz would correspond to a resonant dimension of 50 μm, or even smaller for the overtones, and these length scales cannot be attained in our experimental setup. Consequently, we have an upper cutoff in our systems.

There is also a specific voltage window for the observation of polyhedral drops. As has been seen with mechanical excitation, at the resonant frequency, the drops are deformed and vibrate with the applied frequency. However, in addition, the applied electric field induces interfacial polarization, similar to that observed in dc electrospraying, and the charges can get focused on the antinodes of the polyhedral shape, akin to charge focusing in the Taylor cone. At comparatively lower voltages, capillary forces are dominant and can manage to prevent drop breakup, and polyhedral drop shapes can be retained. At higher voltages, capillary forces can no longer balance polarization, and drop breakup and ejection take place, as seen in Figure 2. The observation is well supported by the balance of Maxwell stress $\varepsilon E^2/2$ by the capillary pressure σ/R at low frequencies,
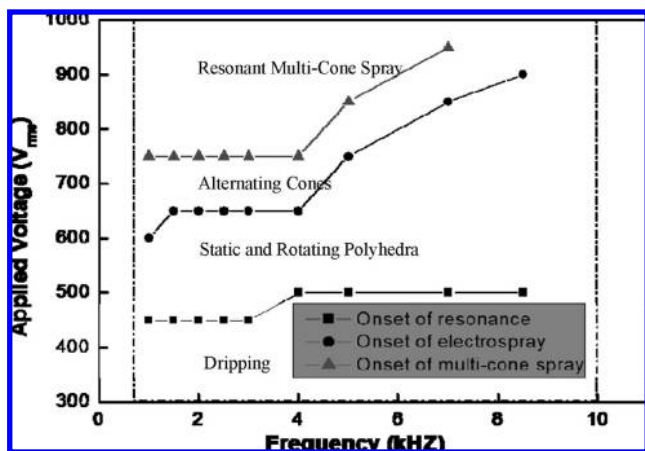
Figure 2. Voltage−frequency diagram, illustrating the voltage window of resonant vibration. The experiments, conducted with acetonitrile showed different modes, increasingly violent, occurring with increasing voltages.

where the Maxwell pressure can be assumed to be independent of applied frequency. For a typical acetonitrile drop of radius $R \sim 1$ mm with surface tension ($\sigma = 19$ mN/m) and density ($\rho_m = 783$ kg/m^3), the required electric field thus translates to an applied root-mean-square voltage $V_{rms} \sim 1.4$ kV. In a similar fashion, balance between gravitational stress $\rho_m g R$ and Maxwell pressure $\varepsilon E^2/2$ defines the transition from dripping to polyhedron regime, which can be shown to occur at $V_{rms} \sim 625$ V. It should, however, be noticed that a discrepancy exists between the experimentally observed voltage for the transition from polyhedron regime to drop pinch off ($V_{rms} \sim 650$ V) and the theoretical voltage obtained by the balance between the Maxwell stress and capillary pressure ($V_{rms} \sim 1.4$ kV). More exact prediction in values can be obtained by solving the governing equations for potential function to obtain the electric field and hence, Maxwell stress. Nevertheless, this scaling argument predicts the relative magnitude of applied potential required to assist the transition from dripping to polyhedron regime and from polyhedron to drop pinch off. We also note the weak increase in voltage for the polyhedra regime with frequency. This trend reflects the fact that the Maxwell forces that deform the drop into polyhedra and the vertices into jets must overcome interfacial capillary forces. As the drop size R decreases with f according to the RL dispersion relationship, the restraining capillary force increase, and larger voltages are necessitated.

Figure 3 shows both the measured and theoretical drop radius calculated from RL dispersion relation at a frequency of 1 kHz as a function of the wave mode number. In fact, the theoretical trend line is very close to a straight line for small mode numbers. Our measurements agree with theoretical values quantitatively in the middle range, while the deviation increases for larger and small mode number at the two ends. At low mode numbers, the drop dimension is not much larger than the needle diameter and the drop is severely constrained. The larger discrepancies at high mode numbers, 5 and 6, are probably because of gravitational effects of the larger drop dimensions. Figure 3b plots the drop radius of the same mode number taken from six independent sets of experiments as a function of the applied frequency f. For fixed mode number n, the droplet diameters is proportional to $f^{-2/3}$, with a theoretical slope of 14 (SI units) for acetonitrile from the RL relation. Collapsing the measured data, gives rise to a slope of 13.7.

At higher voltages, the polyhedra become unstable and transient Taylor cones with liquid ejection appear at the polyhedral vertices in each half-cycle. These transient Taylor cones begin to interact at even higher voltages shown in Figure

4 such that they flicker violently. Figure 4 also compares images between ramified drop fission modes of dc sprays (a), resonant ac sprays with transient Taylor cones (b and c), and nonresonant electrospray (d) without well-defined cones. Unlike its dc counterpart, the cones of resonant ac sprays are not confined to the orifice edges where the electric field is the strongest but are evenly distributed over the entire meniscus, at roughly the antinodes or the vertices of the transient polyhedra. Even though there are multiple transient Taylor cones for resonant ac sprays, the individual cone volume of each cone (Figure 4b and c) can be larger than the dc cone (Figure 4a). Moreover, the onset voltage of multicone spray with ac resonance is found to be lower than its dc equivalent. However, it is also seen that the resonance and transient Taylor cones are favored more at low frequencies and are not observed beyond 10 kHz. As shown in Figure 4d, when the frequency is increased to 8 kHz, the Taylor cones are replaced by a smooth drop and a single liquid jet is ejected at the tip of the drop as in high-frequency ac electrosprays discussed later.

2.2. High Frequency Behavior. From the discussion on low frequency behavior, it is clear that low frequency spraying is similar to dc electrospraying with an oscillating electric field, with an additional complication introduced due to the matching of the applied frequency with the natural vibrating frequency of free drops. For higher frequencies, we find different meniscus shapes like steady conical shapes, unsteady jets, tip-streaming, oscillating meniscus, etc. which suggest that the governing mechanism is quite different from dc or low frequency ac spraying.[16] In the following sections, we discuss the different spraying modes and attempt to provide a mechanistic framework for the high frequency spraying behavior. An ionic liquid, butylmethylpyrrolidinium bis(trifluoromethylsulfonyl) imide (Solvent-Innovation, 98% purity), is used for varying the conductivity of the organic liquid sample. By varying the concentration of the ionic liquid, a group of solutions with different conductivities, varying between 1−10 μS/cm, are prepared. These conductivity values are quite low and can change within this range easily if any contamination takes place; consequently, experiments are performed directly after making the samples and fresh sets are made for every experimental run.

For pure alcohols, viz. ethanol, there are three main spraying modes observed: field accelerated dripping, steady conical meniscus mode, and a discharge assisted ejection. The spraying mode is determined by the applied potential difference. At voltages lower than $\sim$4 kV$_{p-p}$ (kilovolt, peak to peak) dripping takes place, which is accelerated by the applied field. At voltages higher than $\sim$6 kV$_{p-p}$ corona discharge[17−19] becomes visible at the needle tip with the appearance of a bluish glow. This assists the ejection of drops periodically from the needle. Bounded by these two spraying regimes, a stable conical meniscus is observed which does not alternate with the applied frequency but shows temporal growth.

An additional spraying mode is observed at applied frequencies between 15−30 kHz, just before the occurrence of the conical spraying mode. The meniscus is not perfectly stable and localized waves originate at the meniscus tip, with frequencies around 500 Hz, which is much lower than the applied frequency. We shall henceforth call it the oscillating meniscus mode. With increasing applied frequency, the conical meniscus becomes perfectly steady and so we move from the oscillating mode to the conical mode.

With increasing conductivity, the lower frequency bound for the oscillating meniscus mode and the conical mode both increased and new spraying modes became visible at lower
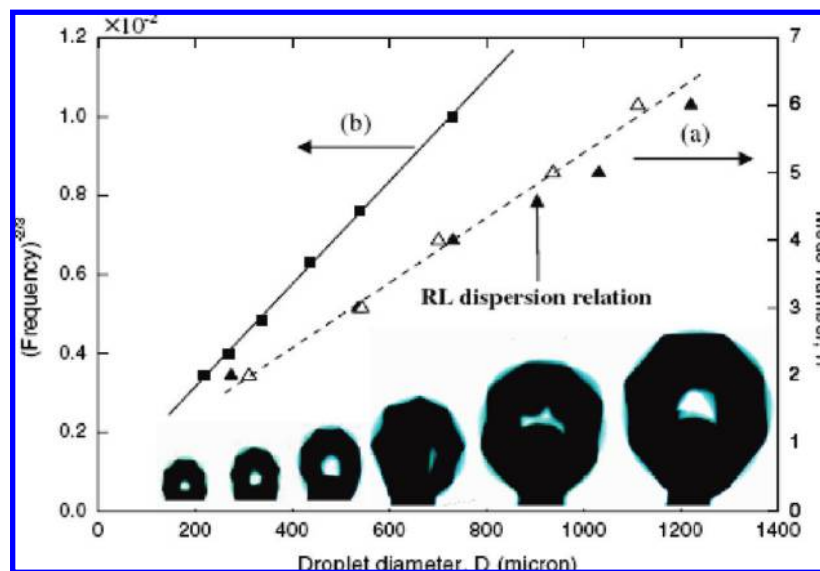
Figure 3. (a) Observed resonant drop diameter (solid triangles) and calculated resonant drop diameter (empty triangles) as a function of the mode number ($f = 1$ kHz). The dashed line is the theoretical curve of RL dispersion relationship. (b) Observed resonant drop diameter as function of applied frequency ($n = 4$). The solid line is a linear regression of the data. The images are polyhedra with the same mode under, $n = 4$, under different applied frequencies: from left to right $f = 5$, 4, 3, 2, 1.5, and 1 kHz, respectively. Acteonitrile was used for the experiments.
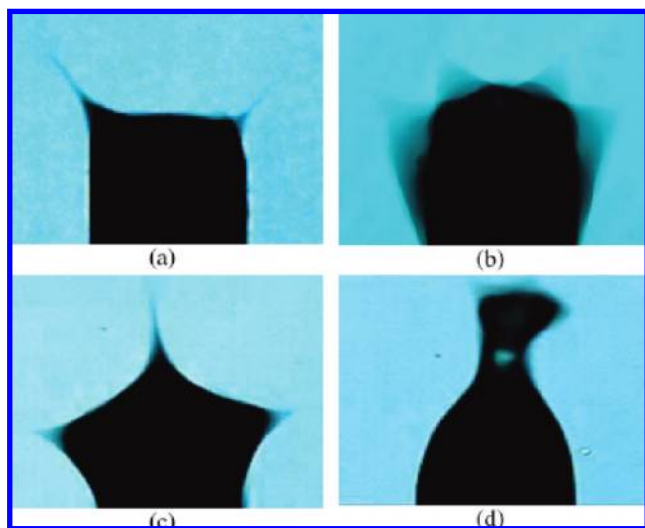
Figure 4. Comparison between dc and resonant and nonresonant ac electrosprays. The separation distance between the needle and ground electrode is 10 mm. (a) Typical dc ramified mode at 3 kV. (b and c) Resonant ac electrosprays at 900 V_{rms}, $f = 1$ and 3 kHz. (d) Typical ac electrospray at 1.2 kV_{rms}, $f = 8$ kHz. The experimental liquid was acetonitrile.

frequencies. Before the onset of the oscillating mode, a tip streaming mode and elongated-fast dripping mode appeared. With pure ethanol these modes are difficult to observe, since the oscillating mode appears as early as 15 kHz, and below ~10 kHz, resonance effects are dominant, as discussed previously. Consequently the frequency window available for the tip streaming and elongated-fast dripping modes is very small.

As the conductivity is increased the frequency at which the oscillating and conical meniscus modes appear is also increased and consequently there is a larger window which makes the observation of tip-streaming and elongated-fast dripping modes possible. This is shown in Figure 5 where schematic voltage–frequency diagrams for three samples, pure ethanol with low conductivity and ethanol doped with different amounts of ionic liquid resulting in a sample with intermediate conductivity and a sample with high conductivity, are depicted. The introduction

of additional spraying modes and the variation in the onset frequency of different modes due to increasing conductivity can be seen.

The actual variation in the onset frequency of the oscillating mode with changing liquid conductivity is shown in Figure 6. We can see that with increasing conductivity the oscillating mode occurs at higher applied frequencies. The experimental results also point toward a linear proportionality between the transition frequency and the liquid conductivity. The onset frequency of the oscillating mode has been reported since a very distinct change in meniscus behavior is observed at the juncture when the meniscus changes from the elongated-fast dripping mode to the oscillating mode.

These distinctions suggest some mechanistic differences between high frequency ac spraying and dc/low frequency ac spraying. The origin of these differences might be explained by the additional dominant timescale for these experiments, the half-period of the applied field where the frequency ranges from 15 to 190 kHz. The half-period then corresponds from 33 to 2.6 μs. For the sprayed ethanol, the charge relaxation time is ~3.1 μs. The insufficient time available for charge relaxation and the continuous growth of the conical meniscus suggest that some preferential charge entrainment is taking place every period leading to a progressive accumulation of charge in the liquid bulk resulting in a growing meniscus Hence, it is necessary to understand the interplay and relative importance of the different timescales and to relate some unique features of ac sprays to such interactions. To achieve this end, experiments are carried out by varying the liquid conductivity as well as the frequency and magnitude of the applied field and observing the liquid meniscus in each scenario. In addition to varying the relative magnitude of the timescales to decipher their importance, this also allows us to obtain an all inclusive phase diagram of the spraying behavior depending upon the liquid properties and applied field.

3. High Frequency Electrosprays

As is clear from the preceding discussion, the high frequency ac electrospraying behavior is quite different from dc electrospraying and points toward an unusual charging discharging
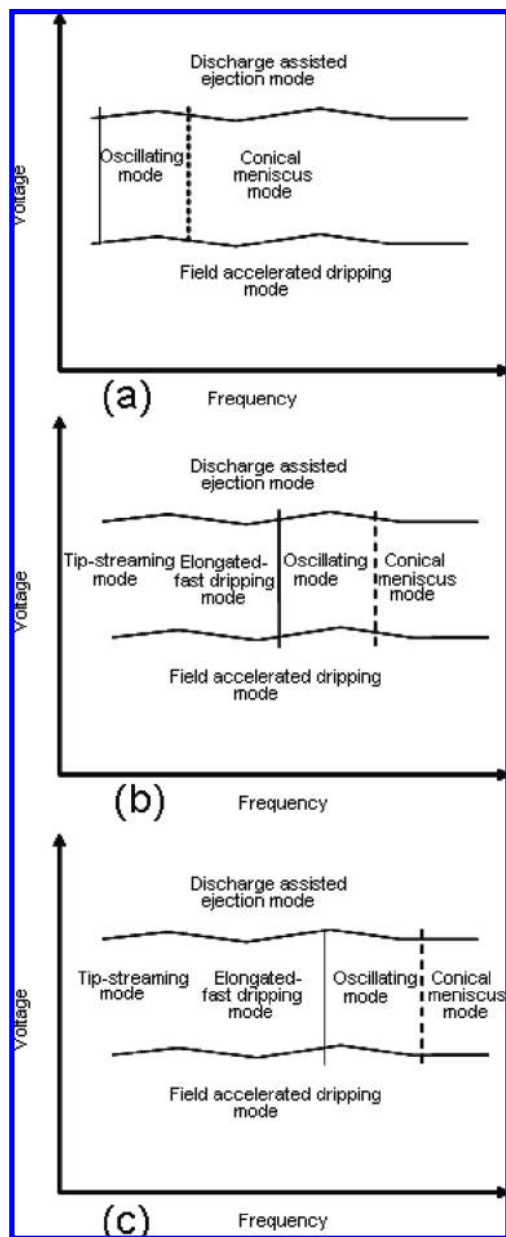
Figure 5. Phase space indicating the appearance of additional modes with increasing conductivity of pure ethanol sample in part a to ethanol doped with ionic liquid in part c. Figure 5b corresponds to an intermediate conductivity of doped ethanol sample. Comparison between parts b and c suggests that the oscillating meniscus and conical meniscus modes are shifted to higher frequencies as the sample conductivity is increased.

behavior. Hence in the following sections, we will discuss this phenomenon in greater detail and examine its different facets.

3.1. Different Spraying Modes. We shall now discuss the different spraying modes observed. We have limited our discussion to the modes occurring between approximately 4−6 kV$_{p-p}$, since the dripping mode below 4 kV and the discharge mode above 6 kV are driven by phenomena that is independent of liquid conductivity and polarization. In fact, we have verified that the change in conductivity does not affect the frequency−voltage window for these modes.[20]

(i) Tip-Streaming. In the mode classified as tip-streaming, small fragments are torn intermittently from the liquid meniscus. The dimension of these fragments is much smaller (∼5 μm) than the entire liquid meniscus, which has a radial dimension comparable to the diameter of the electrospray needle (300 μm). This mode is more prevalent at lower applied frequencies (<30
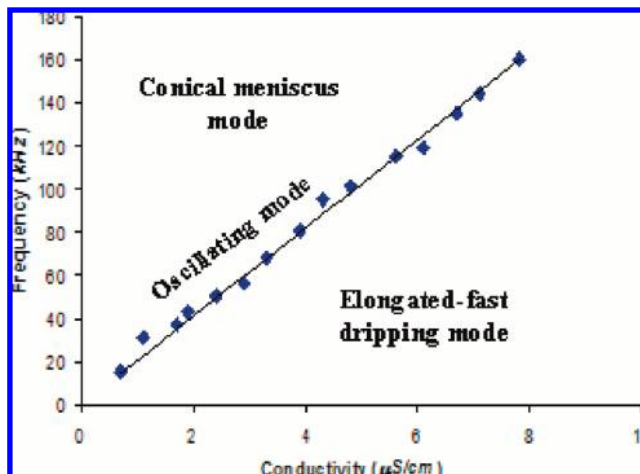

Figure 6. Onset frequency of the oscillating mode as a function of conductivity. With increasing conductivity of the ethanol sample, the onset of oscillating mode is delayed to higher frequencies. The change in the onset frequency is also approximately linear with the sample conductivity.
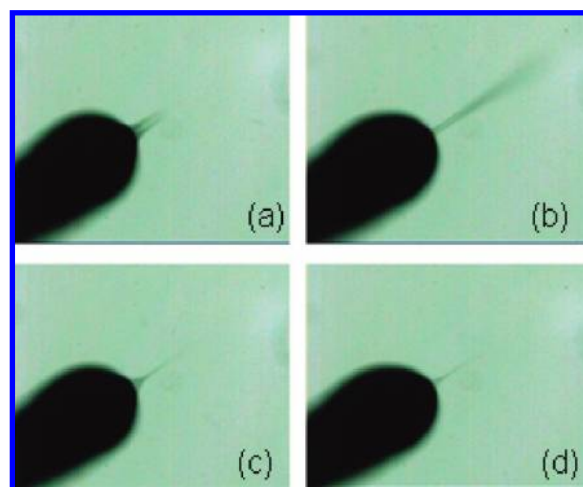

Figure 7. Tip Streaming: successive images at 0, 0.5, 1, and 1.5 ms at an applied frequency of 13 kHz for ethanol.

kHz) than at higher frequencies. The frequency of ejection events in this mode varies with the applied frequency and initially increases with frequency, until approximately 20 kHz. Beyond this frequency, elongated-fast dripping mode starts appearing along with tip-streaming and the behavior at the meniscus tip changes. The tip-streaming mode is shown in Figure 7. The shapes of the meniscus as well as the dimensions of the ejected fragments and the fact that the ejection frequency increases with applied frequency suggest that this mode shares some similarities with dc spraying and particularly the micro-dripping and cone-jet modes and is comparable to dc spraying with a varying field.

(ii) Elongated-Fast Dripping Mode. In the elongated-fast dripping mode, liquid accumulates near the needle tip initially and then it is stretched to form a cylindrical jet with velocities as high as 1 m/s. This jet is then detached at the needle tip to form drops approximately 50−100 μm in dimension. In contrast to the steady jet in dc electrospraying where a thin (∼1 μm) but steady jet emanates from the cone-tip, this jet is unsteady, retracting and reforming subsequently, and much larger in radial dimension. It still suffers from the capillary/inertial instabilities for jets as it pinches off at the needle to form drops the size of the needle. With the advent of this mode, ejection events decline with frequency and then become approximately constant after
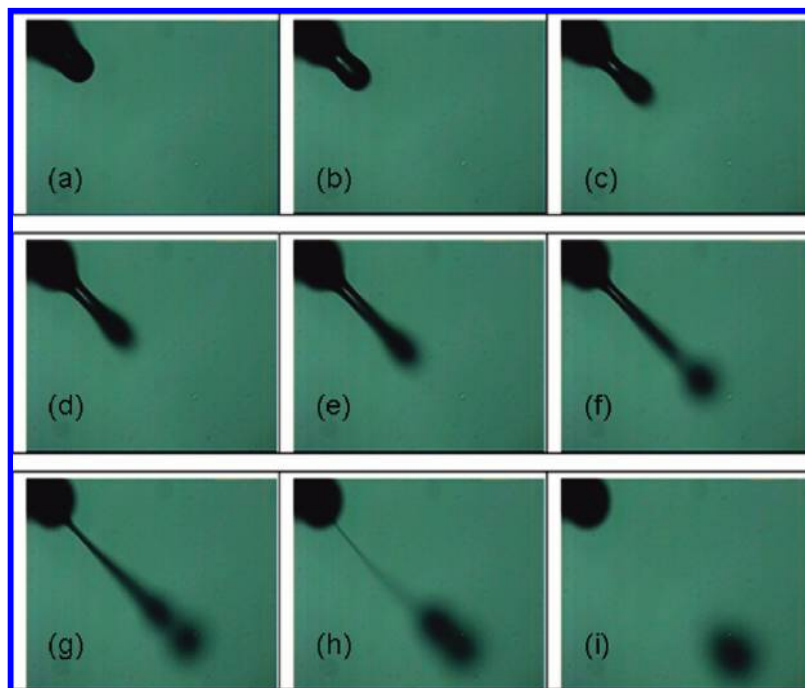
Figure 8. Elongated-fast dripping: successive images at 0, 2.2, 2.4, 2.6, 2.8, 3.2, 3.6, 3.8, and 4 ms at an applied frequency of 40 kHz for a glycerine−ethanol (20−80%, by volume) mixture.
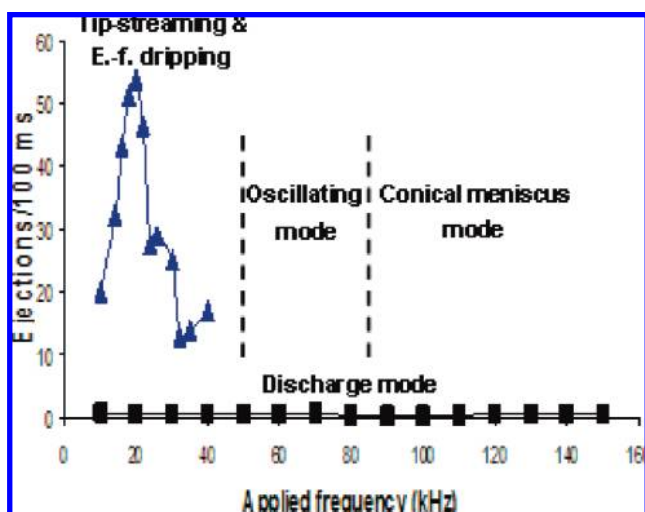
Figure 9. Variation in ejection frequency with applied frequency for a doped sample, where ethanol has been doped with the ionic liquid to achieve a conductivity of approximately 2.2 μS/cm. The triangles correspond to the tip-streaming and jetting modes, while the squares represent the discharge assisted ejection mode.

~30 kHz, where the elongated-fast dripping mechanism becomes predominant. The elongated-fast dripping mode is shown in Figure 8. Unlike the tip-streaming mode, the ejection frequency for this mode does not depend upon the applied frequency, but varies between 100−1000 Hz.

In Figure 9, we have shown the variation in ejection frequency for a doped sample where the oscillating meniscus mode appears at 50 kHz. The initial increase and then decrease of the ejection events points to the initial dominance and then decline of the tip-streaming mode because of the occurrence of elongated-fast dripping. For comparison, the ejection frequency in the discharge assisted ejection mode is also shown as a function of the applied frequency. This mode is a result of corona discharge occurring due to high voltage being applied at the needle tip. Ejection frequency for this mode remains constant throughout,

showing that liquid conductivity has no influence on gas discharges, which is expected.

(iii) Oscillating Mode. The transition from the elongated-fast dripping mode to the oscillating mode is very sharp. This is because in the elongated-fast dripping mode drop pinch off at the needle tip takes place. In contrast, the oscillating mode seems to be immune to capillary/inertial instabilities and the jet does not pinch off at the needle tip at all. Instead it vibrates, and whatever ejection takes place occurs from the tip of the meniscus, when it is at its fully elongated position. The meniscus is shaped like a cylinder with a spherical tip. The cylindrical part of the meniscus in the oscillating mode mostly does not pinch off but oscillates with time. The radius of the cylinder consequently oscillates in a single cycle of vibration, attaining its largest value when the length is smallest and its least value when the cylinder is fully elongated. However, the radius can increase over a longer time scale due to accumulation of liquid from the needle. Also, the ejection from the meniscus tip does not take place every period, and the ejection frequency is less than the oscillation frequency. There can be either single or multiple drop formation from a single ejection event. Total meniscus breakup, akin to the elongated-fast dripping mode, is unfavorable in the oscillating mode. However like the elongated-fast dripping mode, the meniscus vibration frequency in the oscillating mode is totally independent of the applied frequency or the liquid conductivity. It depends only on the diameter of the meniscus and decreases with increase in this length scale. Figure 10 shows one cycle of the oscillating meniscus mode at 81 kHz.

During the course of an experiment, the meniscus diameter generally increases as more and more liquid accumulates there; subsequently, the oscillation frequency shows a gradual decline. This suggests that liquid viscosity is playing an important role in this behavior. In fact this can be clearly deduced from Table 1, where the oscillation frequency and the meniscus diameter have been provided along with the applied electrical frequency and the inverse momentum diffusion time scale. The inverse momentum diffusion time scale is v/l^2 where v is the liquid
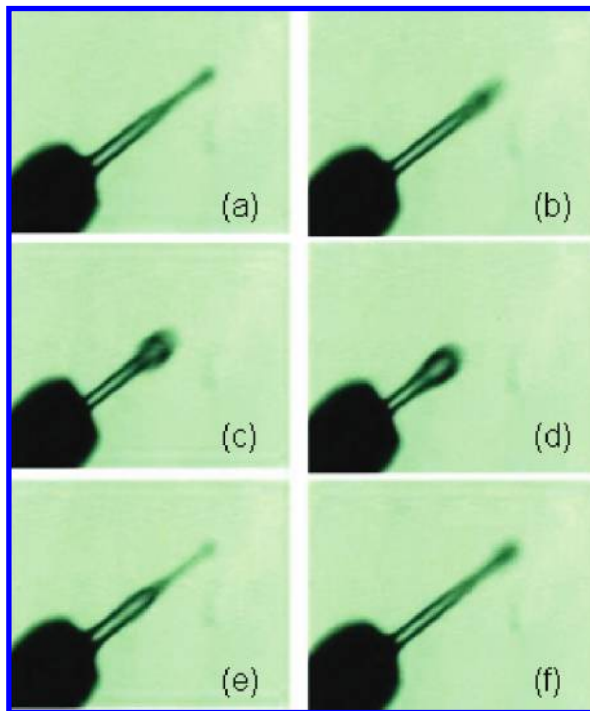
Figure 10. Oscillating meniscus mode: one oscillation of the meniscus, successive images at 0, 0.5, 1, 1.5, 2, and 2.5 ms at an applied frequency of 81 kHz and for doped ethanol with conductivity 3.9 μS/m.

Table 1. Timescales in Oscillating Meniscus Mode for Some Doped Ethanol Samples, with Varying Conductivity

meniscus diameter (μm)	applied frequency (kHz)	oscillation frequency (Hz)	inverse momentum-diffusion time (Hz)
66.7	55	312.5	342
70	81	307.7	310
75	135	295.1	270.2
91.7	55	230.8	180.8
97.1	101	192.8	161.2

momentum diffusivity (1.52×10^{-6} for ethanol) and l is the drop length scale, taken as the diameter of the liquid cylinder at its most compressed state. The measurement of oscillation frequency has been carried out during intervals when droplet ejection from the meniscus tip has ceased, since ejection can vary the oscillation frequency.

As is clear from Table 1, the applied frequency and the oscillation frequency differ by approximately 3 orders of magnitude. Besides, there is no observable correlation between the two. In contrast, the inverse momentum diffusion time scale is quite close to the observed oscillation frequency and explains the variation of the experimental frequency with the meniscus diameter. The difference between the two might be due to inaccuracies involved in the measurement of the diameter when the comparatively small meniscus is oscillating at high velocities (~1 m/s). This timescale behavior also explains the observed range for ejection frequencies in the elongated-fast dripping mode.

(iv) Conical Meniscus Mode. This is the final spraying mode observed that occurs after the oscillating meniscus mode with increasing applied frequency. The meniscus takes a conical shape with a thin (~1 μm) jet ejecting from the tip of the conical meniscus, very similar to the dc-cone jet mode. The most obvious discrepancy observed here is the steadiness and growth of this conical shape. Classical dc spraying theory suggests the formation and annihilation of cones every half-cycle, since the polarity of liquid phase charge is changing every half-cycle,
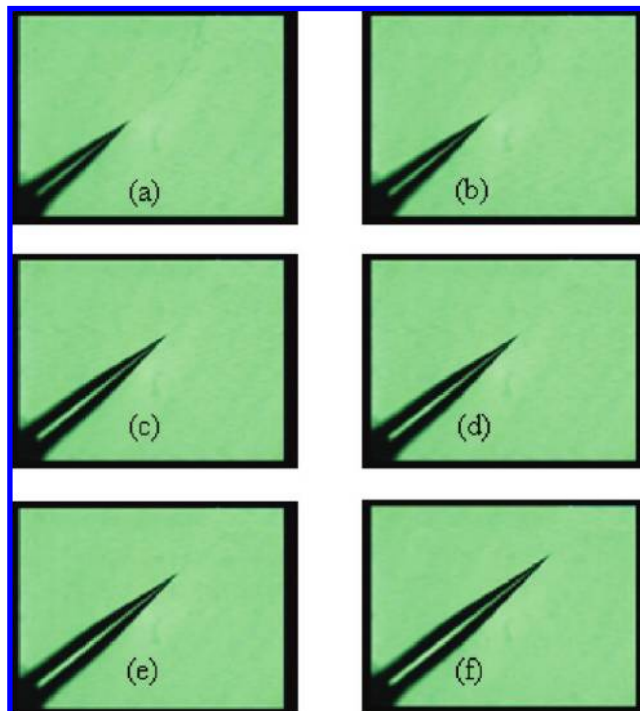
Figure 11. Plot of ac stable cones with a longitudinally growing meniscus at 5 kV$_{\text{p-p}}$ and 95 kHz: successive images, row-wise then columnwise, taken at 0, 2, 4, 6, 8, and 12 s. Pure ethanol was the experimental liquid.

consistent with the behavior observed at low frequencies. However, as our experiments show, the behavior at high frequencies is quite different. Instead of forming and deforming every half-cycle, the cone remains steady. The successive images in Figure 11 also illustrate the longitudinal temporal growth of the meniscus. This elongation of the cone continues, with a constant cone angle, until it becomes unstable at a large aspect ratio (~15:1) and breaks up. Then the meniscus is reformed, and the entire cycle is repeated. To verify that this growth process is an intrinsic feature of the ac spraying mechanism and not due to a flow−rate mismatch between the flows coming out of the cone tip and being supplied by the pump, similar experiments were performed without any imposed flow rate from the pump. But even then, the cone growth continued until the meniscus became very slender and unstable. After pinch-off, if there was some residual liquid at the needle tip, the conical meniscus was reformed and the same process continued, until there was no more liquid remaining. Similar experiments with a dc field did not produce any such growth effect. Due to zero flow from the pump, the dc cone became unsteady and continued to form and break until all the liquid at the needle tip was exhausted. This unsteadiness was a result of the flow rate mismatch because there was a definite amount of liquid being ejected from the cone tip but there was no liquid supply from the pump. Even in this unsteady cone, the aspect ratio remained constant at approximately 1:1 throughout. This demonstrates that the growing meniscus is the effect of the applied ac potential and is limited to high frequency ac spraying. Another important distinction between the dc cone jet mode and the ac conical regime is the half angle of the cones. The half angle of the dc cone for ethanol was found to be ~47° which is very close to the Taylor angle of 49.3°. However for the ac case, the angle is ~11° which is significantly less than the dc case, although the same liquid has been used.[21,22] The cone angle remains approximately constant throughout the applied frequency window.

This was seen for both pure organic samples and samples with increasing conductivity. However, no upper bound in

frequency was reported, if any, for the observation of these conical modes as we could not generate high voltages at frequencies beyond 200 kHz. It should also be noticed that the cones obtained are perfectly stable but not perfectly steady, in the sense that the cone tip retains its shape but its length is elongating in time over a period much longer than the ac period.

3.2. Timescale Analysis. From the preceding information, we can find several features that can explain the relevant charging timescales for the ac spraying phenomena. Figure 6 shows the linear increase in the frequency for the onset of oscillating mode with the liquid conductivity. For charging of electrolytes, the relevant time scale is the charge relaxation timescale which describes the gradual discharging of the liquid bulk, until all the residual charge is confined to the surface.

$$\rho = \rho_0 e^{-t/\tau} \tag{ii}$$

where ρ_0 is the initial charge density and ρ is the charge density after time t, while τ is the charge relaxation time $\beta\varepsilon_0/K$. For our case, the relevant timescale is the semiperiod of the applied field, implying that (ii) can be rewritten as

$$\rho = \rho_0 e^{-2K/\beta\varepsilon\omega} \tag{iii}$$

where ω is the applied frequency. Consequently, it is clear that with increasing frequency, there is less time available for the bulk to discharge and it retains a higher fraction of the original charge. However with increasing conductivity, the bulk discharges faster and retains lesser amount of charge. With these arguments and the results of Figure 6, it is clear that the oscillating meniscus has a greater amount of charge than the meniscus in the elongated-fast dripping mode. More importantly, the linearity of the reported curve demonstrates the existence of a threshold amount of charge for the advent of the oscillating meniscus mode, which is independent of the liquid conductivity or the applied frequency. By fitting the experimental results with a straight line, we find that when the period is approximately 20 times the charge relaxation time, the transition from the elongated-fast dripping mode to the oscillating meniscus takes place. Under such conditions, at every half-cycle approximately 0.001% of the bulk charge is unrelaxed. Hence we can say that for the oscillating meniscus to appear, 0.001% of the liquid bulk charge needs to be retained. We also recall that in the oscillating mode there is no pinch-off near the needle tip unlike the elongated-fast dripping mode where the jet pinches off near the needle tip. Consequently, it can be inferred that this transition occurs at a specific charge fraction since the stabilizing effect of charge against the capillary instability prevents breakup of the liquid cylinder and allows for the transition from the elongated-fast dripping to the oscillating mode. The vibrating menisci in the oscillating mode are the precursors to the steady growing conical menisci which appear at higher frequencies; it is clear that even more bulk charge needs to be retained for the conical meniscus to appear and grow in length. Evidently, sufficient bulk charge exists with the oscillating mode to suppress the instability for jet breakup. However, this bulk charge does not grow in time and hence cannot elongate the jet. The elongation occurs at even higher frequencies when the ac conical shapes appear, suggesting that an ever-increasing bulk charge is responsible for the ac cone formation and its elongation. This is in complete contrast to the classic cone-jet mode in dc spraying, where the charge in the liquid bulk is relaxed because the charge relaxation time scale is the smallest relevant timescale for that process and the bulk becomes electroneutral.
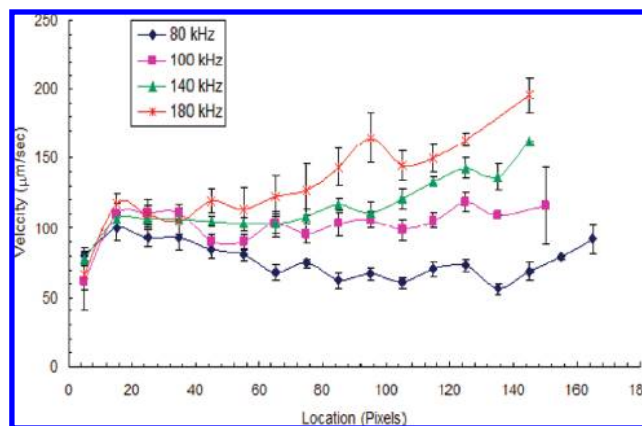
Figure 12. Variation of the cone growth rate with applied frequency for pure ethanol. The cone velocity is plotted at different locations, with the origin placed at the initial position of the cone tip.

4. Proposed Mechanism

The above discussion clarifies the distinction between dc and high frequency ac spraying. However, it does not explain why steadily growing ac cones appear in the first place, since the applied high frequency should form either cones every half-cycle or no cones at all. The appearance of these cones might be a result of charge entrainment, i.e. ions of specific polarity not totally discharging every period, as a result of which that specific charge progressively builds up and ultimately when it crosses a certain threshold, the meniscus changes to a cone. The amount of charge buildup would be sensitively dependent upon the relaxation timescale since discharging of the bulk depends upon that. This would explain why cones appear only when the period of the applied field is a specific fraction of the charge relaxation time scale. This charge buildup model can also explain the growth that is observed in high frequency ac cones and not in dc cones. Since there is an entrainment of specific polarity charge every period, so there is a temporal growth in the charge density in the bulk, and Coulombic repulsion forces the cones to grow. Ultimately when the aspect ratio of the cone becomes too high, capillary instability eventually destroys the conical meniscus, and then the entire process is repeated. For dc cones, there is no charge buildup, and consequently, the conical meniscus does not vary with time. Similarly, the absence of a cone and jet elongation in the elongated-fast dripping and oscillating modes suggests that the bulk charge does not grow in time for these modes.

4.1. Experimental Evidence. This postulation of charge entrainment and growth is further supported indirectly by two very distinct experimental measurements and a mass spectrometric analysis. Since we postulate that the growth of the cones is due to charges of a specific polarity accumulating every period, then the growth rate of the cones must be very strongly correlated with the applied frequency. For higher applied frequencies, the corresponding period is shorter, and so more periods occur for any specific amount of time, as compared to a lower applied frequency. Therefore, greater charge accumulation should be possible at higher frequencies. Consequently, the growth rate of the cone should be directly proportional to the applied frequency.[22] This was observed experimentally as shown in Figure 12, where we have plotted the measured cone growth rate at different distances away from the original cone tip, at different frequencies. It can be seen that, at higher frequencies, the cone grows at a faster rate.

The second indirect evidence comes from the observation of a specific charge in the drops generated during the elongated
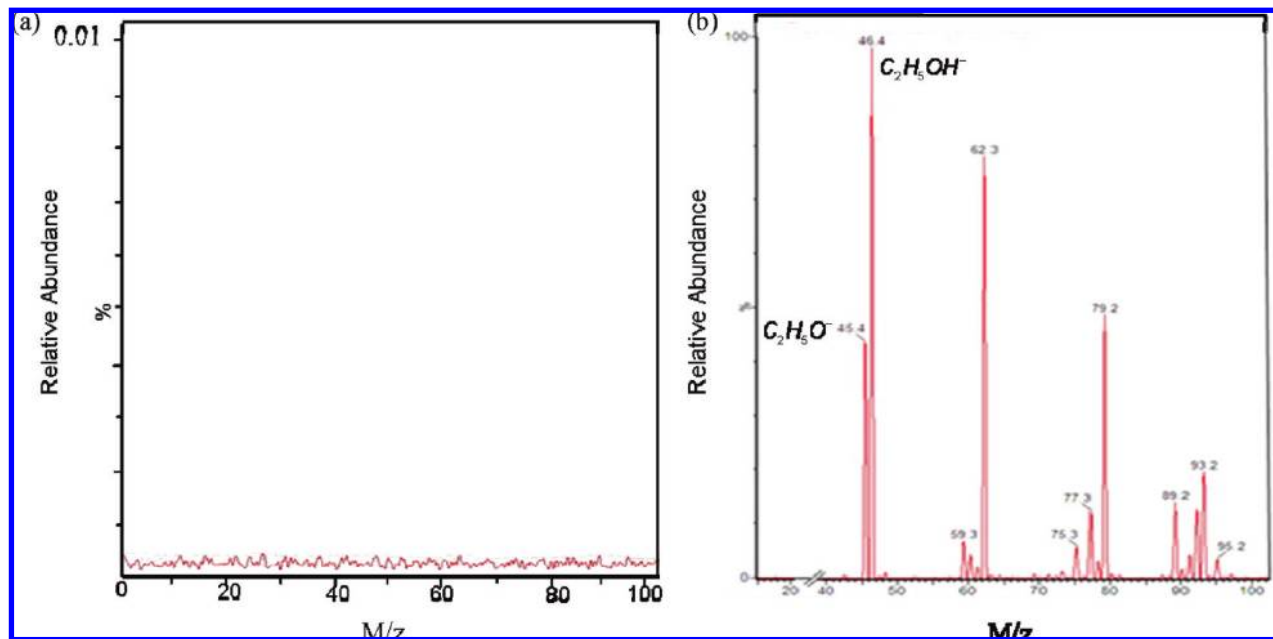
Figure 13. (a) Positive-mode mass spectrometry and (b) negative-mode mass spectrometry of ethanol solution under an ac field of 80 kHz and 4 kV_{p-p}.

fast-dripping mode as well as the cone jet mode. Precise estimation of charge by direct charge measurement techniques was hampered in ac electrospraying, because of the presence of large background noise. We measured the charge in the drops obtained from the elongated fast-dripping mode by studying their deflection in a dc electric field, and for the drops obtained in the cone-jet mode, mass spectrometry was used.

When the drops generated from the elongated fast-dripping mode were passed between parallel electrodes across which a dc field is applied, we observed a continuous deflection of the drops toward the anode despite the periodic reversal in polarity of the applied ac field.[23] The same phenomenon was observed if the polarity of the dc electric field on the parallel plates was reversed, thus suggesting that the drops carry a negative charge. It did not matter whether the live voltage was positive or negative; the drops were always deflected toward the anode. This was not true when mechanical methods were used to generate the microdrops instead of the ac electric field, ruling out that deflection is due to charges being induced due to the effect of the dc field. We also verified that the drop deflection is due solely to Coulombic attraction and not dielectrophoretic motion[24] by using disparate electrode sizes in order to create a nonuniform dc electric field. Since there was no specific preference in the attraction of the drops toward a low or high field region and the drops continued to be deflected toward the anode, drop motion due to positive or negative dielectrophoresis can be eliminated.

To further investigate the identity of the anions ejected from the ac electrospray, mass spectrometry on the ac electrospray of ethanol was carried out. While in the positive mode mass spectrometry, only background noise was observed (Figure 13a), distinct peaks corresponding to ethoxide and ethanol anion radical were observed in the negative mode (Figure 13b). The other peaks that were observed in the negative mode mass spectrum were identified via tandem mass spectrometry and were found to be strongly correlated to ethoxide ion and were possibly formed by its oxidation in presence of ambient air after ejection.

To explain this peculiar phenomenon of ejection of negatively charged species from ac electrosprays, we consider the dis-

sociation of ethanol into ethoxide and a proton that occurs near the tip of the cone, where the electric field is maximum due to the formation of cusp. During the cathodic half-cycle, the high mobility protons relax away from the tip of cone while the ethoxide anion, whose mobility is an order of magnitude less than that of proton, stay in the vicinity of the tip during the anodic half-cycle. Before these anions could relax, the polarity of the applied ac electric field reverses resulting in the net build of negative charge in the cone every cycle of the ac field. We attribute this nonequilibrium charging mechanism to be responsible for the anomalous physical features of the ac cone viz. a half-cone angle of ~11° and a continuous longitudinal growth which are in direct contrast to a stationary dc Taylor cone with a half-cone angle ~49°.

4.2. Theoretical Model. For the theoretical confirmation of the above mechanism, the anionic charge that is accumulated in the cone is represented by the axisymmetric surface charge distribution σ_s. The mutual normal electrostatic repulsive pressure between this charge distribution is proportional to σ_s^2, and hence to sustain a conical structure, it should balance the singular normal capillary pressure, which scales as r^{-1} near the tip of the cone, where r is the radial coordinate of the spherical coordinate system. Using this scaling argument for surface charge distribution, the total electrostatic self-energy of the charged cone is evaluated and is given by $E(\rho,\theta) = [9Q^2/(64\pi^3\varepsilon_l)][I(\theta)/r]$, where $Q = \int \sigma_s \, dA$ is the total charge that lies on the surface of the cone and $I(\theta)$ is the shape factor that accounts for the conical geometry and is given by

$$I(\theta) = \int_0^1 \int_0^{r_2} \int_0^{2\pi} \int_0^{2\pi} \times$$

$$\frac{\sqrt{r_1 r_2}}{\sqrt{r_1^2 + r_2^2 - 2r_1 r_2[\sin^2\theta \cos(\phi_1 - \phi_2) + \cos^2\theta]}} \times$$

$$d\phi_1 \, d\phi_2 \, dr_1 \, dr_2 \quad \text{(iv)}$$

Due to the conservative nature of electric force field, the electrostatic forces that act within the liquid cone are given by $F = -\nabla E$ where E is the electrostatic self energy of the charged cone. Using this expression for force, the electrostatic forces within the charged conical structure are computed.
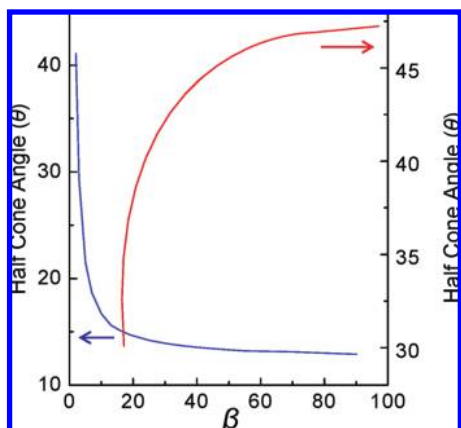
Figure 14. Comparison of theoretical values of half-cone angle for dielectric ac and dc cones.

The normal stress equilibrium at the interface, in conjunction with the tangential repulsive forces with the axial capillary force acting at the sharp tip of the cone, yields the final governing equation for the half-cone angle, which is independent of the surface tension of the liquid or any macroscopic length scale.[23]

$$-\frac{\sigma}{r}\left(\frac{1}{I(\theta)}\frac{dI(\theta)}{d\theta}\right) + \frac{\sigma}{r}\left(\frac{2\pi^2}{I(\theta)\sin\theta}\right)\left(\frac{\beta-1}{\beta+1}\right) = \frac{\sigma}{r}\cot\theta \quad (v)$$

where β is the permittivity ratio of the liquid (inner) and outer (gas) phase. The first term in (v) is the normal electrostatic repulsive pressure, while the second term accounts for the Maxwell pressure that arises due to the interaction between the field generated by the negative space charge distribution and the induced charges at the interface due to difference in polarizability of liquid and gaseous phase. The third term indicates the normal capillary pressure that balances the first two electrical stresses.

The solution of (iv) in the permittivity space is shown in Figure 14. In contrast to the increasing trend for the dc cones with β, the half-cone angle for ac electrosprays decreases rapidly and asymptotes to a value of 12.6°. This difference is again a direct consequence of the charging mechanisms responsible for sustaining the conical structure in both dc and ac cones. Whereas in case of a dc cone, the external field polarizes the liquid interface, the electric field from the accumulated space charge within the liquid phase generates the repulsive forces in an ac cone, which in turn balances the surface tension forces to sustain a stable conical meniscus. The theoretical value of 12.6° is in good agreement with the experimental value of ~11° for ethanol, acetonitrile, and isopropanol.[23]

5. Applications

DC electrospraying has been successfully employed as a key soft ionization technique to ionize the biological molecules like proteins.[1] However, its use has been limited to the positive mode due to the high electron discharge that is triggered by the application of negative potential on the electrode. This often leads to the failure of emitter in a nanospray device and signals that are less stable. A variety of methods that have been adopted to avoid the failure of emitter in negative mode include coating the emitter with a dielectric like polyaniline[25] or using an electron scavenger gas like oxygen or SF_6 in the ambient,[1,26] which absorbs excessive electrons. Negative mode mass spectrometry is particularly useful for ionizing the nucleotides and certain peptides that can readily undergo deprotonation. This has led to the increasing use of MALDI as an ionization

technique for negative mode mass spectrometry for the analysis of oligonucleotides.[27] Nevertheless, negative mode spectrometry using electrospray ionization remains an underutilized tool. Given that the formation of ac electrosprays requires the entrainment of low mobility anions, the high mobility electrons are prevented from being discharged.

This distinct feature of ac electrospray in turn makes it a promising tool for ionizing large negatively charged molecules such as DNA for a negative mode mass spectrometry. In addition to biological applications, ac electrosprays can be used for identification of large chain aliphatic hydrocarbons in jet fuels. The current literature indicates that for the analysis of large chain aliphatic hydrocarbons in jet fuels, the negative mode mass spectrometry leads to better analysis due to better signal strength.[28] This again indicates the potential advantages of ac electrospray as a tool for analysis of jet fuels for industrial applications.

Additionally, using a similar approach, we have found that ac electrospinning shows considerable difference from dc electrospinning[29] and can enhance the applicability of electrospinning.[30−32] Multistranded threads and mesh networks with predetermined morphology can be formed by altering the experimental conditions, which can prove to be very useful for specific applications like fabric weaving and filtration as well as for biomedical applications.[33]

6. Conclusion

It is obvious that using an ac electric field for electrohydrodynamics leads to some fascinating physical phenomena and opens up possibilities for novel applications. The frequency timescale provides a tunable parameter with significant impact on the final outcome of the electrospraying process. The low frequency electrosprays, with multiple Taylor cones, can be used as a high throughput source for generating nanodrops at a rate much higher than a dc Taylor cone and can be employed for variety of applications. The high frequency ac electrosprays, on the other hand, with distinct physical differences as compared to its dc counterpart, viz. a continuously growing meniscus that retains a half-cone angle ~11°, can serve as a new soft ionization technique for negative ion mode mass spectrometry for analysis of several classes of peptides and oligonucleotides. We hope that this review provides a coherent introduction to this field and stimulates further interest.

Literature Cited

(1) Fenn, J. B.; Matthias, M.; Meng, C. K.; Wong, S. F.; Whitehouse, C. M. Electrospray ionization for mass spectrometry of large biomolecules. *Science* **1989**, *246*, 64.

(2) Salata, O. V. Tools of Nanotechnology: Electrospray. *Curr. NanoSci.* **2005**, *1*, 25.

(3) Zeleny, J. The Electrical Discharge from Liquid Points, and a Hydrostatic Method of Measuring the Electric Intensity at Their Surfaces. *Phys. Rev.* **1914**, *10*, 1.

(4) Taylor, G. I. Disintegration of Water Drops in Electric Field. *Proc. R. Soc. A* **1964**, *280*, 383.

(5) Kebarle, P. A brief overview of the present status of the mechanisms involved in Electrospray mass spectrometry. *J. Mass Spec.* **2000**, *35*, 804.

(6) Gomez, A.; Tang, K. Charge and fission of droplets in electrostatic sprays. *Phys. Fluids* **1994**, *6*, 404.

(7) Cole, R. B. Some tenets pertaining to electrospray ionization mass spectrometry. *J. Mass Spec.* **2000**, *35*, 763.

(8) Ganan-Calvo, A. M.; Davilla, J.; Barrero, A. Current and Droplet Size in the Electrospraying of Liquids: Scaling Laws. *J. Aero. Sci.* **1997**, *28*, 249.

(9) Jayasinghe, S. N.; Edirisinghe, M. J. Electric Field driven jetting from dielectric fluids. *App. Phys. Lett.* **2004**, *85*, 4243.

(10) Sato, M.; Takahashi, M.; Awazu, M.; Oshima, T. Production of ultra-uniformly-sized silica particles by applying ac superimposed on dc voltage. *J. Electrostat.* **1999**, *46*, 171.

(11) Borra, J. P.; Tombette, Y.; Ehouarn, P. Influence of electric field profile and polarity on the mode of EHDA related to electric discharge regimes. *J. Aero. Sci.* **1999**, *30*, 913.

(12) Yeo, L. Y.; Lastochkin, D.; Wang, S. C.; Chang, H.-C. A New ac Electrospray Mechanism by Maxwell-Wagner Polarization and Capillary Resonance. *Phys. Rev. Lett.* **2004**, *92*, 133902.

(13) Ramos, A.; Morgan, H.; Green, N. G.; Castellanos, A. ac electro-kinetics: a review of forces in microelectrode structures. *J. Phys. D* **1998**, *31*, 2338.

(14) Lamb, H. *Hydrodynamics*; Cambridge University Press: New York, 1932.

(15) Bazant, M.; Squires, T. M. Induced-Charge Electrokinetic Phenomena: Theory and Microfluidic Applications. *Phys. Rev. Lett.* **2004**, *92*, 066101.

(16) Wang, P.; Maheshwari, S.; Chang, H. C. Polyhedra formation and transient cone ejection of a resonant microdrop forced by an ac electric field. *Phys. Rev. Lett.* **2006**, *96*, 254502.

(17) Yeo, L. Y.; Hou, D.; Maheshwari, S.; Chang, H.-C. Electrohydrodynamic surface microvortices for mixing and particle trapping. *Appl. Phys. Lett.* **2006**, *88*, 233512.

(18) Hou, D.; Maheshwari, M.; Chang, H.-C. Rapid Bioparticle Concentration and Detection by Combining a Discharge Driven Vortex with Surface Enhanced Raman Scattering. *Biomicrofluidics* **2007**, *1*, 014016.

(19) Yeo, L.; Friend, J. R.; Griffin, D. R. Electric Tempest in a teacup: The tea leaf analogy to microfluidic blood plasma separation. *Appl. Phys. Lett.* **2006**, *89*, 103516.

(20) Maheshwari, S.; Chang, H.-C. Effects of bulk charge and momentum relaxation times on ac electrospraying. *J. App. Phys.* **2007**, *102*, 034902.

(21) Maheshwari, S.; Chang, H.-C. Anomalous conical menisci under an ac field-departure from the dc Taylor cone. *App. Phys. Lett.* **2006**, *89*, 234103.

(22) Maheshwari, S. Anomalous Microfluidic Behavior near Singular Interfaces. PhD Dissertation, University of Notre Dame, 2008.

(23) Chetwani, N.; Maheshwari, S.; Chang, H.-C. Universal cone angle of ac electrosprays due to net charge Entrainment. *Phys. Rev. Lett.* **2008**, *101*, 204501.

(24) Pohl, H. A. *Dielectrophoresis*; Cambridge University Press: New York, 1978.

(25) Bigwarfe, P. M., Jr.; White, T. P.; Wood, T. D. Polyaniline-coated nanoelectrospray emitters: performance characteristics in the negative ion mode. *Rapid Commun. Mass Spec.* **2002**, *16*, 2266.

(26) Cole, R. B.; Harrata, A. K. Charge-state distributuion and electric-discharge suppression in negative-ion electrospray mass spectrometry using/chlorinated solvents. *Rapid Commun. Mass Spec.* **1992**, *6*, 536.

(27) Griffin, T. J.; Smith, L. M. Single-nucleotide polymorphism analysis by MALDI-TOF mass spectrometry. *Trends Biotech.* **2000**, *18*, 77.

(28) Rostad, C. E.; Hostettler, F. D. Profiling Refined Hydrocarbon Fuels Using Polar Components. *Environ. Forensics* **2007**, *8*, 129.

(29) Maheshwari, S.; Chang, H.-C. Assembly of Multi Stranded nanofiber Threads, through ac Electrospinning. *Adv. Mater.* **2009**, *27*, 349.

(30) Buchko, C. J.; Chen, L. C.; Shen, Y.; Martin, D. C. Processing and microstructural characterization of porous biocompatible protein polymer thin films. *Polymer* **1999**, *40*, 7397.

(31) Wang, X.; Drew, C.; Lee, S.-H.; Senecal, K. J.; Kumar, J.; Samueleson, L. A. Electrospun nanofibrous membranes for Highly Sensitive Optical Sensors. *Nano Lett.* **2002**, *2*, 1273.

(32) Yoshimoto, H.; Shin, Y. M.; Terai, H.; Vacanti, J. P. A biodegradable nanofiber scaffold by electrospinning and its potential for bone tissue engineering. *Biomaterials* **2003**, *24*, 2077.

(33) Yeo, L.; Gagnon, Z.; Chang, H.-C. ac Electrospray Biomaterial Synthesis. *Biomaterials* **2005**, *26*, 6122.